Electron-energy-loss-spectroscopy near-edge fine structures in the iron-oxygen system

C. Colliex
IBM Research Division, Almaden Research Center, 650 Harry Road, San Jose, California 95120 and Laboratoire de Physique des Solides, Bâtiment 510, Université de Paris–Sud, 91405 Orsay, France

T. Manoubi
Laboratoire de Physique des Solides, Bâtiment 510, Université de Paris–Sud, 91405 Orsay, France

C. Ortiz
IBM Research Division, Almaden Research Center, 650 Harry Road, San Jose, California 95120
(Received 18 October 1990; revised manuscript received 24 April 1991)

We report an electron-energy-loss-spectroscopy study of the characteristic oxygen K and iron $L_{2,3}$ edges in FeO, Fe_3O_4, α-Fe_2O_3, and γ-Fe_2O_3 thin films. Data have been processed for quantitative elemental analysis and for detailed comparison of the different fine structures (energy position and width as well as relative intensities). Oxygen edge profiles are sensitive to the local bonding and symmetry properties on the excited anion. The features of the prepeak at the onset are governed by the $3d$ components in the hybridized unoccupied pd wave functions. They can be described in a molecular-orbital scheme and depend on the first coordination shell. Oscillations at higher energies are interpreted in terms of backscattering from the next coordination shells. The intense white lines on the iron $L_{2,3}$ edges are due to strong $2p^6 3d^n \rightarrow 2p^5 3d^{n+1}$ excitations, and the recorded changes of relative intensity (or branching ratio) are predominantly governed by strong Coulomb and exchange interactions on the excited cation.

I. INTRODUCTION

The Fe-O system in thin-film configurations is a very interesting material system to study because of its complexity and potential technological applications. In this paper we will investigate some properties of four different compounds: FeO, Fe_3O_4, γ-Fe_2O_3, and α-Fe_2O_3. The first oxide, FeO, has a NaCl structure with a tendency to be defective in Fe. It is antiferromagnetic. Fe_3O_4 and γ-Fe_2O_3 are ferrites with inverse spinel structure, whereby the oxygen ions form a fcc lattice and the Fe ions occupy tetrahedral and octahedral sites. The ion spins couple antiferromagnetically in the A and B sublattices, whereby there is a final magnetic moment because of a higher occupancy of B sites. Because of their structural similarities, these two oxides are difficult to distinguish in electron spectroscopy.[1] Only techniques sensitive to the polarization of the spin, such as spin-polarized electron photoemission, have been successful in differentiating them. However, these can only monitor the surface region, which, in most of the cases, is known to be not representative of the thin-film structure.[2] Finally, α-Fe_2O_3 has a hexagonal structure with oxygen close packing of the same density as for the ferrites, however, with a slightly different stacking. It is thermodynamically the most stable compound. It is antiferromagnetic, but it may show a small magnetic moment due to spin canting. The goal of this paper is to use electron-energy-loss spectroscopy (EELS) for the investigation of the electronic structure of these different compounds in the Fe-O system. More specifically, we have studied the changes occurring on the oxygen K edge and iron L edges for each specimen, which was identified by diffraction techniques *in situ* in the electron microscope column. EELS within the electron microscope offers a unique combination of such 1-eV energy resolution for edges between 500 and 800 eV and of good spatial resolution so that it can be performed on submicrometer crystalline grains. As a large set of data has thus been available, various theoretical interpretations have then been reviewed in order to extract some arguments confirming or bringing new contributions to the understanding of the recorded fine structures.

II. MATERIALS: PREPARATION AND CHARACTERIZATION

The films are deposited by reactive rf sputtering in an S-gun magnetron system. The target is iron doped with 1.25 at. % osmium. The substrates are Si(100) wafers to perform magnetic, optical, and x-ray characterization and carbon-coated mica for the transmission-electron-microscopy studies. A planetary holder is used with a fixed 60 rpm rotation speed. Because of this dynamic feature, the monitoring of the substrate temperature has to be performed by a thermocouple located near the rear-side of the holder. The sputtering gas is argon and the reactive gas is oxygen. The flow rates are regulated so that the argon rate is fixed to 80 cm^3/s, and the oxygen is varied from 2 to 10 cm^3/s. The FeO phase is obtained for oxygen flows equal or lower than 3 cm^3/s and temperatures lower than 250 °C. The pure Fe_3O_4 phase is found in the experimental window of O_2 flow of 3–9 cm^3/s. By annealing the Fe_3O_4 sample in air at 275 °C, the metasta-

ble γ-Fe_2O_3 phase can be obtained because both compounds have the same structure, i.e., inverse spinel. The thermodynamically stable α-Fe_2O_3 phase is obtained by annealing Fe_3O_4 in air at temperatures equal to or higher than 450 °C. We used both x-ray and electron diffraction to determine which oxides were present in the specimens and to select samples with single phase and no preferential orientation. This study has shown that the γ phase, which contains ordered Fe vacancies, can only be obtained within restricted experimental conditions.

Only the spinel-based oxides have a final magnetic moment **M**, and their magnetic properties can therefore be studied in order to determine the best deposition conditions.[3] In the case of the Fe_3O_4 phase, the value of the magnetic moment, measured at 20 kG, is very dependent on the deposition conditions in terms of oxygen flow and substrate temperature. For flows higher than 8.5 cm^3/s, the moment drops under 100 emu/cm^3. At the same time, the grain size has an average diameter of 60 Å and superparamagnetism is detected by conversion-electron Mössbauer spectroscopy.[4] This same technique shows, on the other hand, that when the substrate is at room temperature, one observes a reduction of grain size and a large distribution of hyperfine fields, which means a distorted lattice where the *A* and *B* sites are mispopulated. These factors explain that the final magnetic moment is only 240 emu/cm^3.

The thickness of the samples is generally between 50 and 70 nm, and this constitutes a compromise between being able to measure the magnetic and optical properties and, however, not having too much multiple scattering in the EELS study.

III. EELS INSTRUMENTATION

The measurements have been performed with a dedicated scanning transmission electron microscope (STEM, Vacuum Generators HB501) equipped with a Gatan serial energy-loss spectrometer. All spectra are recorded in an image mode, i.e., with a probe of 100-keV incident electrons focused on the specimen surface: The irradiated area depends on the excitation of the three-lens illumination optics and can vary from a minimum diameter of 0.5 nm (with a current of $\simeq 2\times10^{-10}$ A and a half-angle of 7.5×10^{-3} rad) to several tens of nonmeters in a fixed-beam mode. The probe can also be scanned over a broader area in order to reduce the primary dose at the expense of a degradation in spatial resolution. In the present series of experiments, the high spatial homogeneity of the specimens allows us to average the measurements over sizes of a few hundreds of nanometers.

In order to increase the intensity of the signal on core-loss edges, the transmitted beam is collected within a large angle of $\simeq$20 mrad (half-angle measured at the specimen exit surface). A compression factor of $\simeq$5 is applied by the objective post-specimen field before the spectrometer entrance, so that the energy resolution can then be maintained at a 1-eV level for all energy losses up to $=1-2$ keV, i.e., for all edges investigated during this study.[5]

However, the angular distribution of the inelastic electrons, having suffered a typical energy loss $\Delta E=500$ eV, is restricted within a smaller angle, of $\Delta E/2E_0$ (i.e., 2.5×10^{-3} for $E_0=100$ keV). Consequently, when no angular discrimination is achieved in order to enhance the selection of large-angle scattering, the dipole approximation ($qr \ll 1$) is valid for these excitations involving electrons on orbitals of $\simeq$0.1 Å radius.

Spectra are recorded in a serial mode by ramping the beam at the spectrometer exit through a selection slit in front of a standard plastic scintillator-photomultiplicator system capable of single-electron counting. The energy-loss scan is governed by the digital unit control of the STEM, and the energy loss increment and dwell time can be decided by the experimentalist, in order to be conveniently adapted to the problem under investigation: The voltage and intensity power supplies are sufficiently stable to offer the possibility of adding many scans (up to 50 with 20 ms/channel and scan) while maintaining a typical 1-eV resolution on the edge of fine structures—total recording time up to 15 mn.

IV. EELS RESULTS AND DATA PROCESSING

As illustrated in Fig. 1 for the case of α-Fe_2O_3, the useful information contained in an EELS spectrum lies over an extended energy-loss domain from a few eV to about 1 keV. The low-energy-loss range from $\simeq$2 to $\simeq$40 eV corresponds to excitations of the valence-electron population with a combination of interband and collective plasmon modes. At 55 eV there is a clear asymmetric sawtooth profile (generally preceded with a slight bump at 52–53 eV), which corresponds to the iron $M_{2,3}$ edge, i.e., the excitation of the 3*p* iron electrons toward unoccupied *d* states. It does not exhibit great changes from one oxide to another: It nevertheless deserves a refined analysis by itself in order to evaluate the importance of Fano-type effects (interference between discrete and continuum excitations[6,7]) and of atomic collective excitations.[8]

At higher energy losses, the occurrence of atomic-type excitations from deeper atomic shells introduces very clear features superposed over the continuously decreasing background: These are the oxygen *K* edge at about 530 eV and the iron $L_{2,3}$ edge (excitations from the 2*p*

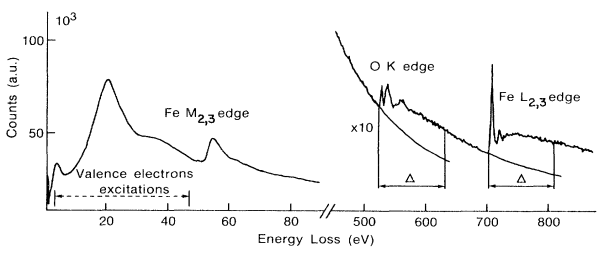

FIG. 1. Complete spectrum of an α-Fe_2O_3 specimen, displaying the different contributions. The extrapolated background is shown below the oxygen *K* and iron $L_{2,3}$ edges. The characteristic signal is measured over an energy window of width Δ for quantification.

TABLE I. EELS elemental analysis of the different iron oxides, using the characteristic O K and Fe $L_{2,3}$ signals: (a) conventional background-subtraction method after Fourier-log deconvolution and (b) new curve-fitting method. See text for further explanations.

[Fe/O]	FeO	Fe_3O_4	α-Fe_2O_3	γ-Fe_2O_3
Method (a)	1.00±0.07	0.75±0.05	0.65±0.04	0.68±0.04
Method (b)	0.99±0.03	0.73±0.02	0.66±0.02	0.66±0.02

subshell) at about 705 eV. The present paper focuses on these edges. The comparison of edge structures originating from different shells was introduced by Fischer,[9] and Grunes has clearly demonstrated its interest for different transition-metal oxides.[10]

A. Concentration-ratio measurements

There are several ways of handling the data concerning the high-energy O and Fe edges (in Fig. 1) in order to extract useful information. The first step is to measure the total characteristic signal S_i for each edge after background subtraction and to use it for quantitative elemental measurements. The basic idea is that this signal is proportional to the number of atoms giving rise to it, when weighted with an appropriate cross-section value.

The conventional analysis method with core-loss edges, as proposed by Egerton, consists of two steps: The first one is the measurement of the characteristic signal $S_i(\alpha,\Delta)$ recorded within an angular acceptance α and integrated over an energy window Δ above threshold. We have used the algorithm developed by Trebbia,[12] which models the background with a power-law mode AE^{-r} over a fitting window Γ preceding the edge and which contains a statistical analysis of the precision on the measurements of S_i. The second step is to calculate

$$\frac{N_{\mathrm{Fe}}}{N_{\mathrm{O}}}=\frac{S_{\mathrm{Fe}}(\alpha,\Delta)}{S_{\mathrm{O}}(\alpha,\Delta)}\,\frac{\sigma_{\mathrm{O}}(\alpha,\Delta)}{\sigma_{\mathrm{Fe}}(\alpha,\Delta)}\ , \tag{1}$$

where the cross sections of interest are obtained from atomic calculations. In a previous paper,[13] we have discussed the influence of selecting either the hydrogenic (Egerton[14]) values or the Hartree-Slater (HS) (Rez[15]) ones. The former ones seem best adapted for use over a large range of Δ values, because the latest parametrization introduced by Egerton in the Sigmal 2 software reproduces at least partially the shape of the differential $L_{2,3}$ cross section with the contribution of the white lines at threshold included. On the other hand, the HS curves exhibit a slightly delayed profile which does not model the white lines, because they only deal with transitions to unoccupied continuum states and do not take into account transitions to the bound states involved in white lines.

In order to improve the accuracy of quantitative measurements for thicker specimens ($t\simeq$inelastic mean free path$\simeq$70–120 nm), signal measurements are performed on deconvoluted spectra. Results for different stoichiometries are shown in Table I, method (a).

In parallel,[13] we have developed an alternative approach for quantitative analysis which consists of simulating the experimental spectrum I_{expt} as a linear combination $F(E)$ of components, such as

$$F(E)=AE^{-r}+\lambda_1\sigma_1(E)+\lambda_2\sigma_2(E)+\ldots\ , \tag{2}$$

where the first term is the background and $\sigma_1(E)$ and $\sigma_2(E)$ are cross sections for the different edges of interest. In this paper we have chosen HS descriptions which

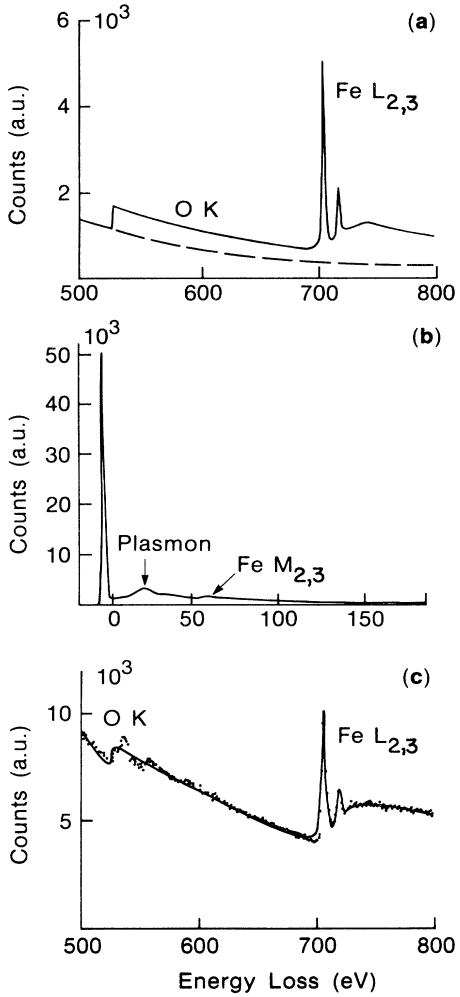

FIG. 2. Curve-fitting method for the quantitative interpretation of the different contributions in an FeO spectrum: (a) simulated spectrum made of a background, an atomic Hartree-Slater cross section for oxygen K and Fe $L_{2,3}$ (corresponding to transitions to continuum states), and two Lorentzian lines for the white lines on the iron edge; (b) low-energy-loss spectrum used for convolution with the model spectrum; and (c) comparison of the simulated spectrum with the experimental one.

correctly describe the transitions to continuum states for both oxygen K edge and iron L edge, and we have added explicit Lorentzian (or Gaussian) terms $L_2(E)$ and $L_3(E)$ for the description of the white lines on the iron edge. Such a model spectrum is shown in Fig. 2(a).

The second aspect of this curve-fitting method is the incorporation of the option of convolving the model profile with the low-energy-loss part $I_l(E)$ of the spectrum [see Fig. 2(b)], before comparison with the real spectrum [see Fig. 2(c)]. It simulates the effect of multiple inelastic scattering and

$$F(E)=[AE^{-r}+\lambda_1\sigma_1(E)+\lambda_2\sigma_2(E)+aL_2(E)+bL_3(E)]*I_l(E)\ . \quad (3)$$

The best solution for all variable parameters $(A,r,\lambda_1,\lambda_2,a,b,\ldots)$ involved in this simulation is obtained through an iterative least-squares fitting routine. For the purpose of quantitative elemental analysis, one evaluates the ratio between λ_1 and λ_2 when introducing σ_{HS} (oxygen) and σ_{HS} (iron) for the σ_1 and σ_2 cross sections.

The results obtained with this method have been gathered in Table I, method (b). The agreement with the expected values is in all cases very satisfactory and confirms that one is capable of discriminating different iron oxide stoichiometries when carefully processing the core-loss EELS data.

B. Oxygen K-edge fine structures

Figure 3 shows the oxygen K spectra, after background subtraction, for the four studied compounds and an energy resolution of $\simeq 1$ eV. There does not seem to exist in the literature such a comparison of edge shapes over a wide energy range extending up to 40–50 eV above threshold. With EELS techniques, Grunes *et al.*[16] have shown a Fe-O oxygen K edge with a clear and intense prepeak at 530 eV before the major contribution at 539 eV. Very recently, Paterson and Krivanek[17] have compared, with an improved energy resolution ($\simeq 0.3$–0.4 eV), the detailed structure over the first 15 eV of the oxygen K edge in the two types of Fe_2O_3. With the development of new and better monochromators for synchrotron radiation in this energy range, x-ray-absorption studies have also been made with a typical 0.5-eV energy resolution over a 20-eV range above threshold for the O-K edge in FeO (Nakai *et al.*[18]), in Fe_2O_3 (with no phase distinction), and in Fe_3O_4 (de Groot *et al.*[19]).

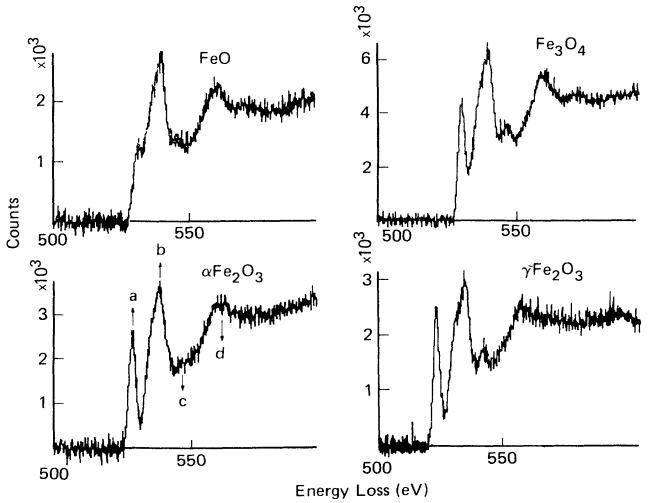

FIG. 3. Comparison of oxygen K spectra after background subtraction for the four compounds studied.

The oxygen K edge displays four distinct features labeled (a)–(d) in the following description (see Fig. 3, α-Fe_2O_3).

(a) is the prepeak below 530 eV whose relative intensity gradually increases from FeO to Fe_2O_3.

(b) is the dominant contribution around 540 eV which remains rather similar for all phases.

(c) is a weaker maximum at $\simeq 545$–550 eV whose position and shape vary between the different compounds, but are similar for the Fe_3O_4 and γ-Fe_2O_3 specimen.

(d) is the major contribution at about 560–565 eV, rather broad and without any characteristic profile. It must be pointed out that in Fig. 3 it has not been possible to achieve multiple-scattering deconvolution because the unsaturated low-loss peak had not been recorded in equivalent conditions. Multiple-loss contributions become actually important at about 30 eV above threshold and can be responsible for noticeable profile modifications for this peak (d) and above.

In order to make more quantitative the comparison between these different spectra, we have tried to decompose the experimental profiles into several terms using a curve-fitting method already described in Refs. 13 and 20. The major goal is to measure selected parameters characterizing the prepeak (a) when compared to the major absorption maximum (b): Its position is defined by the difference in energy with the maximum of peak (b); its width and relative intensity are evaluated when fitting it with a Lorentzian profile. The results are gathered in Table II. Within the accuracy of these measurements, one notes a relative stability of the value of the width and an increase of the intensity by a factor of 2–3 between the FeO and Fe_2O_3 cases, the Fe_3O_4 value being intermediate.

C. Iron L-edge fine structures

Figure 4 shows the iron $L_{2,3}$ spectra after background subtraction for the four oxides under investigation. They all exhibit a rather similar profile with two white lines labeled L_3 and L_2 (i.e., corresponding to excitations from the spin-orbit split levels $2p_{3/2}$ and $2p_{1/2}$) followed by a steady plateau with weak oscillations. After the pioneering work of Bonelle,[21] high-spatial-resolution x-ray-absorption data on these lines for two of the presently studied oxides have only been published recently by Thole and Van der Laan.[22] On the other hand, the $L_{2,3}$ edge in iron has been a favorite feature for EELS studies since the first notice of the anomalous L_3/L_2 white-line ratio in the $3d$ Fe metal by Leapman and Grunes.[23] A

TABLE II. Characteristics of the prepeak (a) on the oxygen K edge.

Relative position with respect to the absorption maximum = energy difference peak (b) − peak (a)	Width of prepeak (a) (in eV)	Relative intensity of prepeak (a) with respect to the absorption maximum (b)
FeO	9.0±0.2	2.3±0.3	0.09±0.01
Fe_3O_4	10.7±0.2	2.3±0.3	0.15±0.01
γ-Fe_2O_3	10.9±0.2	2.1±0.3	0.20±0.01
α-Fe_2O_3	11.0±0.2	2.0±0.3	0.20±0.01

more complete work with a typical 1.5-eV energy resolution by Leapman, Grunes, and Fejes[24] has compared several parameters between the Fe metal and FeO phases: chemical shift of 1.4 eV, reduction of white-line width from 3.5 to 2.4 eV in the oxide, and increase of the intensity $I(L_3)/I(L_2)$ ratio from 3.0 to 4.1 (or from 3.4 to 5.5, depending on the method used for the estimation of the specific white-line weight). Some studies have extended this approach to different oxides: Tafto and Krivanek[25] have analyzed the chemical shift due to valence change ($Fe^{2+} \rightarrow Fe^{3+}$) and to coordination modification (octahedral→tetrahedral) in various complex iron compounds. Otten *et al.*[26] have measured a 2-eV chemical shift from Fe^{2+} to Fe^{3+}. Sparrow *et al.*[27] have confirmed the regular variation of the $I(L_3)/I(L_2)$ ratio through the d-transition series, with a slight increase from 3.3 to 3.6 between FeO and Fe_2O_3. High-energy-resolution studies have also been made by Fink *et al.*[28] on iron and by Paterson and Krivanek[17] on the three oxide phases. The latter study reveals extra fine structures on both L_3 and L_2 lines. Very recently, Krishnan[29] has demonstrated splittings on these white lines, which depend on the oxidation state and coordination number for the iron ion in four model minerals.

We have extracted from our experimental results some more quantitative values for investigating systematic variations between the different specimens. The modelization approach already described in Sec. IV A has been used again, but with emphasis on the shape and intensity of the white lines. When considering Eq. (3), we are now specifically interested by the evaluation of the parameters a and b governing the L_3 and L_2 profiles used for simulating the white lines. Different mathematical laws have been tested, of Lorentz or Gauss type. To improve the fit with lines departing noticeably from simple symmetric shapes, we have also tested the results with two or four components. It must be added that the influence of the model chosen for the underlying transitions to unoccupied states in the continuum is also important for the evaluation of the intensity ratio, because it modifies the magnitude of the intensity fraction attributed to the continuum below the white-line peaks. In general, we have preferred to deal with multiple scattering by convolving the model spectrum with the low-loss spectrum, rather than by applying the fitting procedure on deconvoluted spectra. The results are gathered in Table III. It contains the differences in energy between the two L_3 and L_2 peaks, the widths of these peaks, and the $I(L_3)/I(L_2)$ intensity ratios. For this latter parameter, the two columns, respectively, represent the results of the simplest [2 Lorentz+arctan (continuum functions)] and of the most elaborate (2 Lorentz+Hartree-Slater continuum functions+ convolution) fitting procedures. The result of the best fit is shown in Fig. 5 for the $L_{2,3}$ spectrum of γ-Fe_2O_3.

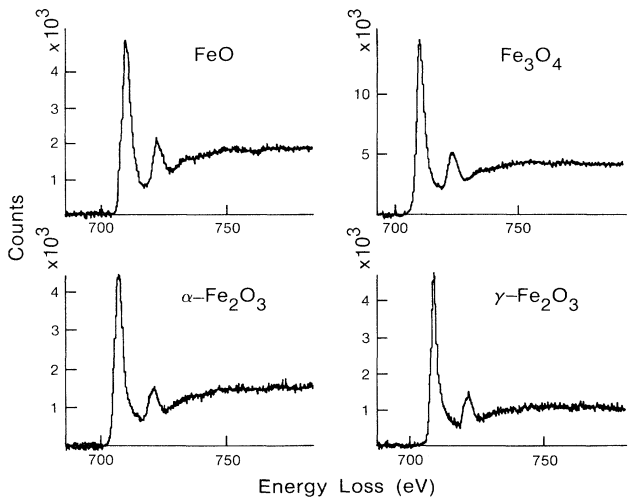

FIG. 4. Comparison of iron $L_{2,3}$ spectra after background subtraction for the four compounds studied.

We confirm the stability of the $(L_3$-$L_2)$ energy difference at about 13.1±0.2 eV for the various phases. It is measured as the difference between the positions of the two Lorentzian curves which model each L_3 and L_2 line. It may deviate from the difference between the position of the experimental maxima when there are slight variations in symmetry or extra-fine structures. We have not performed accurate measurements of absolute-energy-loss values for these peaks, as a consequence of the absence of reliable voltage-measuring devices. Krivanek and Paterson[30] also point out the difficulty in finding a sufficiently accurate standard for an absolute calibration of losses in this energy range.

Concerning the linewidth, we also agree with the previously observed reduction between the metal and oxide, more specially for Fe_2O_3. However, this behavior has not been noticed for FeO, contrarily to the observation by Leapman, Grunes, and Fejes.[24] But in the work of these authors, the detailed structure of the prepeak on the O-K edge is also different from ours and is similar to our

TABLE III. Characteristics of the L_3 and L_2 white lines on the iron L edge. See text for further discussion. The values between brackets for the white-line widths correspond to the simulation of the L_2 peak with two distinct components.

	Relative position of the two white lines = energy difference $E_{L_2}-E_{L_3}$ (eV)	Width of the the white lines ΔL_3 (eV)	ΔL_2 (eV)	Relative intensity of the white lines Method 1	Method 2
Fe	13.2±0.2	3.5±0.2	3.4±0.2	3.8±0.3	
FeO	12.9±0.2	3.9±0.2	3.9±0.2	4.6±0.3	3.9±0.3
Fe_3O_4	13.2±0.2	3.5±0.2	3.6±0.2	5.2±0.3	4.2±0.3
γ-Fe_2O_3	13.2±0.2	2.6±0.2	2.9±0.2 (1.5/2.5)	5.8±0.3	4.4±0.3
α-Fe_2O_3	13.1±0.2	3.2±2.0	3.0±0.2 (1.6/2.4)	6.5±0.3	4.7±0.3

Fe_2O_3 spectrum. It is likely that the specimen, which they call FeO, is rather different from our FeO specimen.

Another net result in the present study is the recorded behavior for the L_3/L_2 intensity ratio which noticeably deviates from the 2:1 value as already noted.[23,24] It confirms more clearly the variation pointed out by Sparrow *et al.*[27] Whatever the method used for measuring the specific weight of each of the two lines, $I(L_3)/I(L_2)$ increases with the valence state. This is the reversed variation with what has been found for Mn oxides (net decrease from MnO to MnO_2). Both of these experimental observations are, however, coherent with an interpretation in terms of d-band occupancy. The $I(L_3)/I(L_2)$ ratio is maximum for $n_d=5$ in the initial state, i.e., for Fe_2O_3 and MnO (see also Sparrow *et al.*[27] and Colliex, Manoubi, and Krivanek[31]).

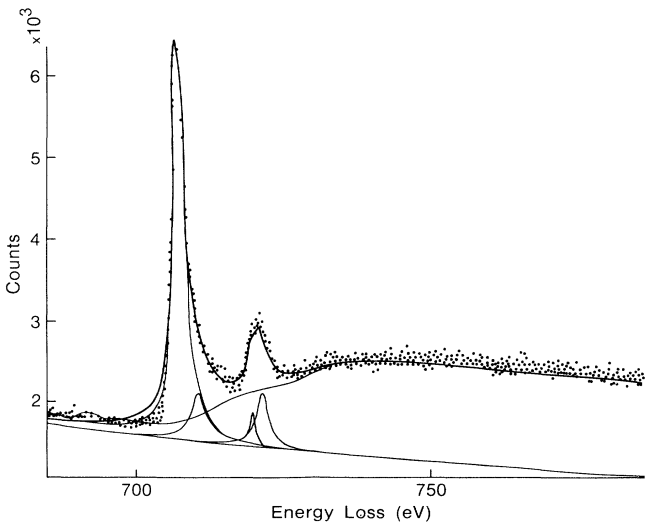

FIG. 5. Best curve fitting for Fe $L_{2,3}$ edge in γ-Fe_2O_3 with two Hartree-Slater cross sections for continuum and four Lorentz functions for white lines and convolution by the low-energy-loss spectrum.

V. DISCUSSION OF THE NEAR-EDGE FINE-STRUCTURE RESULTS

A. Prepeak on the oxygen K edge

In a one-electron (or single-particle) transition model, it is assumed that only one core electron is excited to an unfilled state present in the initial, unperturbed solid. For the excitations investigated in this paper, it amounts to consider either $1s\rightarrow np$ (oxygen K edge) or $2p\rightarrow nd$ (iron $K_{2,3}$ edge) transitions. It would also be valid for the description of the $1s\rightarrow np$ (iron K edge) excitations such as recorded around 7100 eV by Grunes.[10] This assumption neglects exchange interactions between the core hole and final state and fails for the analysis of the $L_{2,3}$ white-line behavior (as will be discussed later on), but constitutes a good starting point for other edges.

Several theoretical models have been developed to describe the final states accessible in a solid-state environment for electrons excited from an atomic core orbital. For a qualitative interpretation of the features observed in the first electronvolts above threshold, molecular-orbital (MO) theory constitutes a useful tool: It calculates the energy and orbitals for a cluster made of a metal ion surrounded by its oxygen nearest neighbors. In the considered oxides, the iron ion lies in a general octahedral environment (O_h symmetry group) for the FeO wustite and the α-Fe_2O_3 hematite (distorted octahedral). In γ-Fe_2O_3, maghemite, $\frac{3}{8}$ of the Fe^{3+} ions are on tetrahedral sites (T_d symmetry troup) and $\frac{5}{8}$ on octahedral sites, while in Fe_3O_4, magnetite, this distribution is $\frac{1}{3}$ on tetrahedral (all Fe^{3+}) and $\frac{2}{3}$ on octahedral sites (one-half being Fe^{2+} and the other Fe^{3+}). A satisfactory starting point therefore consists in calculating the MO's for an iron ion Fe^{2+} or Fe^{3+} in an octahedral environment. The results (respectively, for the clusters $[FeO_6]^{10-}$ and $[FeO_6]^{9-}$), due to Tossell, Vaughan, and Johnson[32] are shown in Fig. 6. The net result is that the $2p$ oxygen and $3d$ iron orbitals combine to give crystal-field split levels t_{2g} and e_g. Moreover, since the iron oxides have ground states with high spin values, a calculation in which the spin-up and -down electrons occupy different orbitals must be performed. The $2t_{2g}\rightarrow 3e_g$ eigenvalue difference is somewhat smaller in the ferrous case (1.7 vs 2.2 eV)

and the spin-orbit splitting is somewhat larger (2.9 vs 2.7 eV). In FeO the highest occupied orbital is the $t_{2g\downarrow}$ containing one electron, and in Fe_2O_3 it is the $3e_{g\uparrow}$ with two electrons. Let us add that in the T_d symmetry group, the hierarchy of energy levels is reversed with lower-lying e states and higher-lying t_2 states. For the evaluation of the separation between t_{2g} and e_g levels (which is also denoted as the ligand-field splitting in the literature), Sugano, Tanabe, and Kamimura[33] propose a "general rule" that it is around 2.5 eV for trivalent ions and approximately half for divalent ions. This analysis has been revisited by de Groot *et al.*[19] who prefer to discriminate between the early and late transition-metal oxides, the early ones with a splitting around 2.5 eV and the late ones with a splitting around 1.2 eV.

This discussion provides an interesting key for understanding the origin and behavior of the prepeak on the oxygen K edge. Following the above description and in accordance with the conclusions by de Groot *et al.*[19] the prepeak (a) corresponds to transitions $1s \rightarrow 2p$ toward the oxygen $2p$ fraction in unoccupied states hybridized with the $3d$ transition-metal orbitals. Moreover, the spatial distribution of the $2p$ fraction is not equivalent on the oxygen and iron sites: It is much more localized on the anion site than on the cation site (see the calculations of percentage spatial distribution in Tossell, Vaughan, and Johnson[32]). Consequently, the strength of the prepeak on the oxygen K edge is, as observed, much higher than on the iron K edge. As a matter of fact, the weak prepeak observed by Grunes[10] on the iron K edge is at least one order of magnitude lower than on the oxygen K edge, when compared to the main absorption maximum. It can then be assigned to quadrupole $1s$-to-$3d$ transitions with low transition-matrix integrals; when the iron environment has no inversion symmetry (tetrahedral site), the dipole-selection rules are relaxed and an increase in the strength of the $1s$-to-$3d$ prepeak is observed (see, for instance, Lytle, Greegor, and Panson[34]).

The absorption maximum (b) can be attributed to transitions to higher-energy vacant states of p symmetry (O $2p$ character in bonds with predominantly $4sp$ transition-metal character). The decrease of the prepeak (a) intensity with respect to peak (b), as measured in Table II, last column, is related to the decrease of the hole population in the $3d$ band as compared to the $4sp$ band: It is a function of the number of $3d$ electrons in the ground state. Extending this interpretation, de Groot *et al.*[19] have pointed out the linear decrease of this prepeak, over the whole transition-metal oxide series, as a function of the number of unoccupied $3d$ states available for mixing with the O $2p$ states. The change that we have found between the Fe_2O_3 and FeO specimens corroborates this statement.

EELS or x-ray data recorded with improved energy resolution confirm this interpretation of the origin of the prepeak. As shown in Fig. 7 due to Paterson and Krivanek,[17] the prepeak in the two varieties of Fe_2O_3 as well as in Fe_3O_4 is itself split into two components, separated by 1.2 eV in α-Fe_2O_3 and by 0.8–0.9 eV in the two other cases. This splitting likely corresponds to the already mentioned t_{2g}-e_g ligand field. The experimental value is about one-half that calculated by Tossell, Vaughan, and Johnson,[32] but agrees with the argument of de Groot *et al.*[19] Moreover, the great similarity of the intensities of the so-called t_{2g} and e_g peaks in the γ-Fe_2O_3 and Fe_3O_4 cases and the difference with the α-Fe_2O_3 case suggest that the detailed behavior is more governed by the change in symmetry (partially tetrahedral versus fully octahedral) than by the exchange splitting (filling of the majority-spin e_g states before the minority-spin t_{2g} states) as suggested by de Groot *et al.*[19]

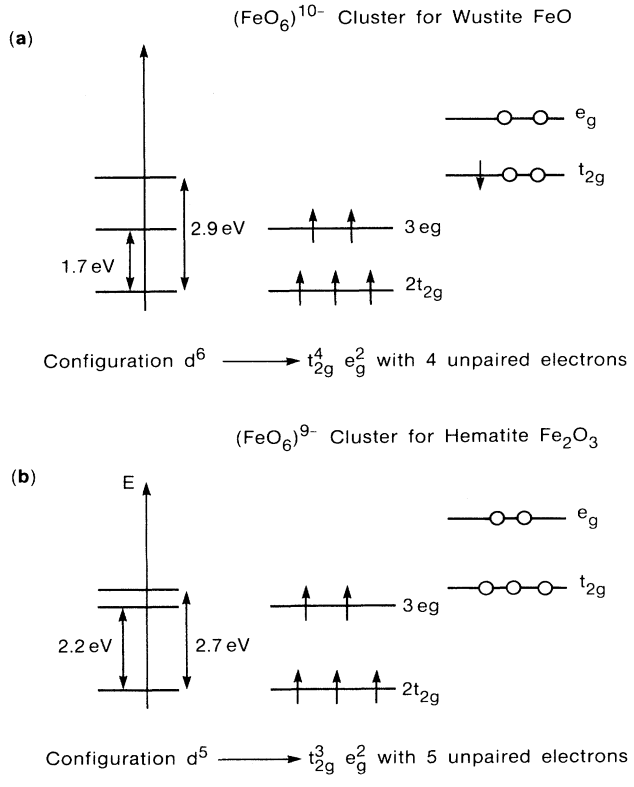

FIG. 6. Molecular-orbital energy diagrams for octahedrally coordinated iron ions: (a) in the wustite FeO, i.e., $(FeO_6)^{10-}$ ion, and (b) in the hematite Fe_2O_3, i.e., $(FeO_6)^{9-}$, from Tossell, Vaughan, and Johnson (Ref. 32).

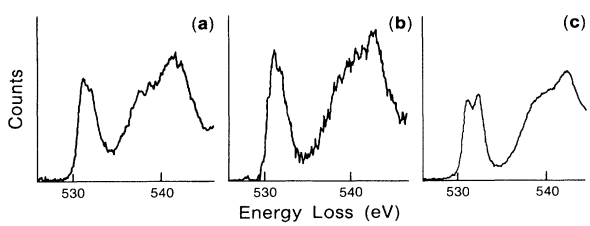

FIG. 7. Comparison of the prepeak splittings on the oxygen K edge recorded with improved energy resolution: (a) Fe_3O_4, (b) γ-Fe_2O_3, and (c) α-Fe_2O_3 [Paterson and Krivanek (Ref. 17)].

B. Secondary effects of symmetry environment on the oxygen K edge

Up to now, we have interpreted the changes on the prepeak visible at threshold in terms of charge transfer and crystal symmetry within the first coordination shell. When considering higher-energy-loss structures, lying between 15 and 30 eV above threshold, we have noticed in Sec. IV B different shapes for the peak labeled (c) lying at about 548 eV, while peak (d) at about 563–565 eV remains rather unaltered (or displays modifications which do not exceed those induced by multiple-loss effects). These variation effects have not been considered by previous investigators.

These oscillations correspond to the well-known ELNES domain [or x-ray absorption near-edge structure (XANES) range in x-ray absorption]. They have to be considered within the multiple-scattering model introduced by Durham, Pendry, and Hodges.[35] The final state for the emitted electron is described as the superposition, on the core-excited site, of an outgoing wave and of the multiple backscattered waves on the successive shells of neighboring atoms. The only detailed XANES-type calculations for oxides which we know are those due to Lindner *et al.*[36] for MgO and to Weng and Rez[37] for MgO, CaO, and SrO. Their calculations, for the simple cubic structure, show that the maxima in the fine structures are induced by the backscattering contribution on the successive shells of oxygen ions which act as reflecting cages around the excited site. In a systematic effort of comparison of XANES spectra through sets of reference specimens, several authors following the initial remark by Stöhr, Sette, and Johnson[38] have identified various XANES features with scattering from first- and higher-neighbor atoms. Lytle, Greegor, and Panson[34] have plotted curves of constant $R^2\Delta E$, where ΔE is the energy above the edge and R the radius of a given coordination shell. Within this description, simple scattering from a shell of neighboring atoms is supposed to be more intense than any multiple scattering. Consequently, the validity of attributing these specific features lying between 15 and 50 eV above threshold to the extended x-ray-absorption fine-structure (EXAFS) or XANES range may be questioned (see Bunker and Stern[39]). It is, however, of secondary importance. In the simple case of MgO, we have been capable of identifying two peaks above the OK edge and two peaks above the MgK edge as due to backscattering oxygen atoms from the successive oxygen shells.[40] Extrapolating this analysis to the more complex present case, peak (d) is likely related to the contribution of the first shell of backscattering atoms and peak (c) to the second one. The observed strong similarity between γ-Fe_2O_3 and Fe_3O_4 and dissimilarity with FeO and α-Fe_2O_3 confirm this interpretation: Up to the second shell of oxygen atoms, the structural environment is similar in both spinel oxides.

C. White lines on the iron $L_{2,3}$ edge

As already mentioned, the one-electron excitation picture fails to interpret several behaviors [width of the peaks, anomalous $I(L_3)/I(L_2)$ ratio] observed on the white lines on the Fe $L_{2,3}$ edge. This is a consequence of the strong overlapping between the $2p$ core orbitals and $3d$ vacant orbitals on the cation site. Consequently, one must consider this type of excitation in terms of $2p^6 3d^n \rightarrow 2p^5 3d^{n+1}$ rather than as a simple $2p \rightarrow 3d$ transition ($n=5$ for Fe^{3+} and $n=6$ for Fe^{2+}). The first step consists in calculating multiplet structures for different ionic configurations. In fact, one should consider the magnitude of the p-d interactions, d-d interactions, spin-orbit interaction of the p hole, and cubic-field term in the solid-state structure. Actually, in the $L_{2,3}$ absorption spectrum, the spin-orbit interaction of the p hole ($\simeq 10$ eV) is one order of magnitude larger than other terms: It is responsible for the general occurrence of a spectrum made of two peaks separated by the spin-orbit interaction. Among the other terms, the p-d Coulomb and exchange interactions play a major role in giving rise to the multiplet satellites which cause a large redistribution of intensities and further splitting of the white lines and therefore induce strong deviations from the 2:1 nominal intensity ratio.

A complete calculation of these strong atomic multiplet splittings was made by Yamaguchi *et al.*[41] Within the strong-field scheme of ligand-field theory, they have

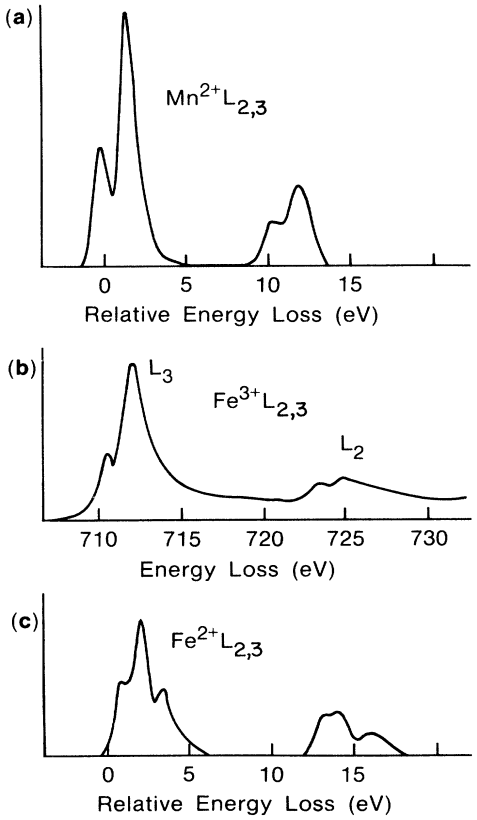

FIG. 8. Comparison of the calculated absorption spectrum for Mn^{2+} (a) and Fe^{2+} (c) cases by Yamaguchi *et al.* (Ref. 41) with the high-energy-resolution Fe $L_{2,3}$ spectrum (b) recorded by Paterson and Krivanek (Ref. 17) for α-Fe_2O_3.

computed all energy matrices of the p-d Coulomb and exchange interactions and of the spin-orbit interaction of p electron for the electron configurations p^5d^{n+1} with $n=0-8$. Their results have been used for comparison with different $L_{2,3}$ absorption spectra for ionic-$3d$-transition-metal compounds (Ohno and Nakai[42]). Figure 8 clearly displays the striking similarity between the high-energy-resolution $L_{2,3}$ spectrum on α-Fe_2O_3 due to Paterson and Krivanek[17] and the calculated absorption spectrum for Mn^{2+} by Yamaguchi *et al.*[41] The three curves have been aligned on the center of the L_3 line. The similarity of the fine structures is quite good between the profiles calculated for Mn^{2+} and measured for Fe^{3+}, which are isoelectronic. On the contrary, the spin-orbit splitting on the $2p$ level is similar between the Fe^{3+} measured and Fe^{2+} calculated curves.

However, these authors have not discussed explicitly the origin of the anomalous behavior of the $I(L_3)/I(L_2)$ ratio (or the branching ratio $Q=I(L_3)/[I(L_2)+I(L_3)]$ as a function of the d-band occupancy. Using an atomic multiconfiguration Dirac-Fock program, Waddington *et al.*[43] have shown that the $I(L_3)/I(L_2)$ ratio increases from subunit values for the first elements ($n=0$) to values considerably higher than 2 for n_d greater than 5. However, they have not explained the critical changes with valency observed around the center of the series. Other calculations, taking into consideration the superposition of the different contributions of atomic and solid-state nature, have been made by Zaanen *et al.*,[44] Thole and Van der Laan,[22] and de Groot *et al.*[45] They are very successful in explaining in detail the spectra recorded for $n_d=0$ (i.e., K^+, Ca^{2+}, Sc^{3+}, and Ti^{2+}) in the O_h symmetry. For more complex electronic configuration, the detailed profiles have not yet been fully reproduced theoretically. However, some very useful rules in relationship with the evolution of the branching ratio can be deduced from the work of Thole and Van der Laan.[22] They show the relative influence of the crystal-field ($10Dq$), spin-orbit (ξ_d), and bandwidth (w) parameters on the branching ratio of the high-spin ground state of $3d$-metal compounds in octahedral symmetry. The maximum in the medium of the $3d$-transition-metal oxides series would correspond to a situation in which the above parameters could be ranked as

$$10Dq > \xi_d > w \ .$$

D. Information about the local magnetic moment

Several authors have pointed out the relation between the value of the branching ratio Q and local magnetic moment. In a study of the EELS fine structure in amorphous magnetic iron alloys, Morrison *et al.*[46] have noted that the $I(L_3)/I(L_2)$ white-line ratio behaves similarly to the reduced iron moment $\mu=\mu_x/\mu_{Fe}$. Basically, they have related them through the number of holes on the two subbands $d_{5/2}$ and $d_{3/2}$: The ratio $h_{d_{5/2}}/h_{d_{3/2}}$ decreases from 1 to 0 for a series of alloys Fe_xGe_{1-x} ($0.2\leq x\leq 0.6$). Further examples of a similar behavior have been recorded. When comparing chromium metal and chromium in $Cr_{20}Au_{80}$ with a strong spin-up state and a localized moment of $4\mu_B$ on the chromium atom, the Cr Q ratio increases from $\simeq 1.5$ in pure Cr to 2.5 in $Cr_{20}Au_{20}$.[47] In an amorphous $Fe_{30}Y_{70}$ alloy,[48] the reduced $I(L_3)/I(L_2)$ ratio (2.3) as compared to pure iron (3.4) provides another evidence of the reduced magnetic moment.

In the present work we can also use the formula

$$\frac{h_{d_{5/2}}}{h_{d_{3/2}}}=\frac{1}{6}\left[\frac{5}{2}\frac{I_{L_3}}{I_{L_2}}\frac{E_{L_2}}{E_{L_3}}-1\right], \tag{4}$$

due to Morrison *et al.*[46] to calculate the ratio of available holes on the two d subbands. We find an increase of $h_{d_{5/2}}/h_{d_{3/2}}$ from $\simeq 1.5$ for FeO to 2.4 for γ-Fe_2O_3, which could also be connected to an enhanced local magnetic moment from a low-spin to a high-spin state on the excited iron ion. Though this comparison must be considered with great caution because the core-hole excitations are screened differently in metals and ionic insulators, it provides hints for further experimental and theoretical investigations: Fine-structure studies on the $L_{2,3}$ edge in $3d$-transition-metal systems may evolve as a useful tool for studying local magnetic properties.

VI. CONCLUSION

A detailed EELS investigation of the fine structures appearing on the K oxygen edge and L iron edge has been performed on four different iron oxides with well-characterized structures. The observed changes have been analyzed in terms of variations for the final states accessible in the excitations involving different initial core orbitals. Electronic properties related to the partial filling of the d band have been shown to be responsible for the behavior of a distinct prepeak on the oxygen K edge. On the other hand, more complex multiplet-splitting effects on the cation site have been evoked for explaining the observed anomalous $I(L_3)/I(L_2)$ ratio. Finally, structural effects have also been considered to interpret the origin of further oscillations occurring at higher energies above threshold, in the typical XANES-EXAFS energy domain.

ACKNOWLEDGMENTS

The authors thank G. Castillo (IBM, San Jose) for his technical assistance in the sample deposition. The Laboratoire de Physique des Solides is "Unité Associée au Centre National de la Recherche Scientifique LA 002."

[1]C. R. Brundle, T. J. Chuang, and K. Wendelt, Surf. Sci. **68**, 459 (1977).
[2]M. Aescklimarin, G. L. Bona, F. Meier, M. Stampanoni, G. Zampien, and H. C. Siegman, Appl. Phys. Lett. **49**, 824 (1986).
[3]C. Ortiz, G. Lim, M. M. Chen, and G. Castillo, J. Mater. Res. **3**, 344 (1988).
[4]C. Ortiz, C. Hwang, A. H. Morrish, and X. Z. Zhou, J. Mater. Res. **5**, 824 (1990).
[5]O. L. Krivanek, T. Manoubi, and C. Colliex, Ultramicroscopy **18**, 155 (1985).
[6]U. Fano, Phys. Rev. **124**, 1866 (1961).
[7]R. E. Dietz, E. G. MacRae, Y. Yafet, and C. W. Caldwell, Phys. Rev. Lett. **33**, 1372 (1974).
[8]G. Wendin, in *EXAFS and Near Edge Structure,* edited by A. Bianconi, L. Incoccia, and S. Stipeich, Springer Series in Chemical Physics Vol. 27 (Springer-Verlag, Berlin, 1983), p. 29.
[9]D. W. Fischer, J. Appl. Phys. **41**, 3561 (1970).
[10]L. A. Grunes, Phys. Rev. B **27**, 2111 (1983).
[11]R. F. Egerton, *EELS in the Electron Microscope* (Plenum, New York, 1986).
[12]P. Trebbia, Ultramicroscopy **24**, 399 (1988).
[13]T. Manoubi, M. Walls, M. Tencé, and C. Colliex, Microsc. Microanal. Microstruct. **1**, 23 (1990).
[14]R. F. Egerton, Ultramicroscopy **4**, 169 (1979).
[15]P. Rez, Ultramicroscopy **9**, 293 (1982); P. Rez, Ultramicroscopy **28**, 16 (1989).
[16]L. A. Grunes, R. D. Leapman, C. N. Wilker, R. Hoffmann, and A. B. Kunz, Phys. Rev. B **25**, 7157 (1982).
[17]J. H. Paterson and O. L. Krivanek, Ultramicroscopy **32**, 319 (1990).
[18]S. Nakai, T. Mitsuishi, H. Sugarawa, H. Maezawa, T. Matsukawa, S. Mitani, K. Yamasaki, and T. Fujikawa, Phys. Rev. B **36**, 9241 (1987).
[19]F. M. de Groot, M. Grioni, J. C. Fuggle, J. Ghijsen, G. A. Sawatzky, and H. Petersen, Phys. Rev. B **40**, 5715 (1989).
[20]T. Manoubi, M. Tencé, and C. Colliex, Ultramicroscopy **28**, 49 (1989).
[21]C. Bonnelle, Ann. Phys. (Paris) **1**, 439 (1966).
[22]B. T. Thole and G. Van der Laan, Phys. Rev. B **38**, 3158 (1988).
[23]R. D. Leapman and L. A. Grunes, Phys. Rev. Lett. **45**, 397 (1980).
[24]R. D. Leapman, L. A.Grunes, and P. L. Fejes, Phys. Rev. B **26**, 614 (1982).
[25]J. Tafto and O. L. Krivanek, Phys. Rev. Lett. **48**, 560 (1982).
[26]M. T. Otten, B. Miner, J. H. Rask, and P. R. Buseck, Ultramicroscopy **18**, 285 (1985).
[27]T. G. Sparrow, B. G. Williams, C. N. Rao, and J. M. Thomas, Chem. Phys. Lett. **108**, 547 (1984).
[28]J. Fink, T. Müller-Heinzerling, B. Scheerer, W. Speier, F. U. Hillebrecht, J. C. Fuggle, J. Zaanen, and G. A. Sawatzky, Phys. Rev. B **32**, 4899 (1985).
[29]K. M. Krishnan, Ultramicroscopy **32**, 309 (1990).
[30]O. L. Krivanek and J. H. Paterson, Ultramicroscopy **32**, 313 (1990).
[31]C. Colliex, T. Manoubi, and O. L. Krivanek, J. Electron Microsc. **35**, 307 (1986).
[32]J. A. Tossell, D. J. Vaughan, and K. H. Johnson, Am. Mineral. **59**, 319 (1974).
[33]S. Sugano, Y. Tanabe, and H. Kamimura, *Multiplets of Transition Metal Ions in Crystals* (Academic, New York, 1970).
[34]F. W. Lytle, R. B. Greegor, and A. J. Panson, Phys. Rev. B **37**, 1550 (1988).
[35]J. P. Durham, J. B. Pendry, and C. H. Hodges, Solid State Commun. **38**, 159 (1981).
[36]T. Lindner, H. Sauer, W. Engel, and K. Kambe, Phys. Rev. B **33**, 22 (1986).
[37]X. D. Weng and P. Rez, Phys. Rev. B **39**, 7405 (1989).
[38]J. Stöhr, F. Sette, and A. L. Johnson, Phys. Rev. Lett. **53**, 1684 (1984).
[39]G. Bunker and E. A. Stern, Phys. Rev. Lett. **52**, 1990 (1984).
[40]T. Manoubi, Ph.D. dissertation, Oray, 1989.
[41]T. Yamaguchi, S. Shibuya, S. Suga, and S. Shin, J. Phys. C **15**, 2641 (1982).
[42]Y. Ohno and S. Nakai, J. Phys. Soc. Jpn. **54**, 3591 (1985).
[43]W. G. Waddington, P. Rez, I. P. Grant, and C. J. Humphreys, Phys. Rev. B **34**, 1467 (1986).
[44]J. Zaanen, G. A. Sawatzky, J. Fink, and W. Speier, Phys. Rev. B **32**, 4905 (1985).
[45]F. M. de Groot, J. C. Fuggle, B. T. Thole, and G. A. Sawatzky, Phys. Rev. B **41**, 928 (1990).
[46]T. I. Morrison, M. B. Brodsky, N. J. Zaluzec, and L. R. Sill, Phys. Rev. B **32**, 3107 (1987).
[47]D. M. Pease, S. D. Bader, M. B. Brodsky, J. I. Budnick, T. I. Morrisson, and N. J. Zaluzec, Phys. Lett. **114A**, 491 (1986).
[48]T. I. Morrison, C. L. Foiles, D. M. Pease, and N. J. Zaluzec, Phys. Rev. B **36**, 3739 (1987).